Systematics of nuclear ground state properties in $^{78-100}$Sr by laser spectroscopy

F. Buchinger and E. B. Ramsay*
Foster Radiation Laboratory, McGill University, Montréal, Canada

E. Arnold, W. Neu, R. Neugart, and K. Wendt
Institut für Physik, Universität Mainz, Mainz, Federal Republic of Germany

R. E. Silverans, P. Lievens, and L. Vermeeren
Instituut voor Kern-en Stralingsfysika, Leuven University, Leuven, Belgium

D. Berdichevsky,† R. Fleming, and D. W. L. Sprung
Physics Department, McMaster University, Hamilton, Ontario, Canada

G. Ulm‡
The ISOLDE Collaboration, CERN, Geneva, Switzerland
(Received 22 February 1990)

Hyperfine structures and isotope shifts of strontium isotopes with $A=78$ to $A=98$ and $A=100$ were measured by collinear fast beam laser spectroscopy. Nuclear spins, moments and changes in mean square charge radii are extracted from the data. The spins and moments of most of the odd isotopes are explained in the framework of the single particle model. The changes in mean square charge radii are compared with predictions of the droplet model and of Hartree-Fock-plus-BCS calculations. For the isotopes in the transitional regions below and above the $N=50$ shell closure, the inclusion of quadrupole zero point motion in the Droplet model describes part of the observed shell effect. An additional change in the surface region of the charge distribution at spherical shape is suggested by the microscopic model. Furthermore, we propose that the isotopes ^{78}Sr and ^{80}Sr may show an unusual shape-sharing structure, with different mean deformations in the ground and 2_1^+ excited states.

I. INTRODUCTION

Strontium, with $Z=38$ protons, belongs to the family of elements close to the $Z=40$ subshell closure which exhibit a rapid variation of nuclear ground state properties as a function of the neutron number towards both sides of the line of beta stability. In these regions, the theoretically well documented strong ground state deformations, as well as predictions of shape isomerism,[1-5] have motivated extensive nuclear spectroscopy investigations. The experiments carried out so far have mainly concentrated on a detailed study of level structures and on measurements of reduced $E2$ transition probabilities.[6-8] They have established experimentally the regions of deformation which peak in the Z,N plane at $Z=38$, $N=38$, and at $Z=38,40$; $N=62$, only a remarkably short interval of 12 neutron numbers away from the spherical region around $N=50$. The results underline the competition and reinforcement of the shell gaps present in the single particle spectrum for neutrons and protons at (N,β) or $(Z,\beta)\approx(40,0)$, $(38,+0.4)$, $(36,-0.4)$, and $(34,-0.3)$ (Refs. 4, 7, 9, 10, and 11) and their influence on the nuclear shape.

This influence was also studied systematically through laser spectroscopy experiments in rubidium (Rb, $Z=37$).[12] The measurements provide spins, moments, and changes of mean square charge radii ($\delta\langle r^2\rangle$) between $A=76$ and $A=98$ and give coherent data which connect the two zones of strong deformation via the regions of transitional and spherical nuclei near the $N=50$ shell closure.

We have undertaken a similarly extensive study of nuclear ground state properties in strontium (Sr, $Z=38$) by fast beam laser spectroscopy. With our investigation of the hyperfine structures (hfs) and isotope shifts (IS) between $A=78$ and $A=100$, we have extended considerably the previous laser spectroscopy studies in this element, which cover mainly the isotopes close to the major neutron shell closure and the transitional nuclei on the neutron deficient side.[13-16] For sensitivity reasons our measurements were carried out in the ionic (Sr II) $5s\,^2S_{1/2}-5p\,^2P_{3/2}$ ($\lambda=407.9$ nm) transition which is also considered most reliable for the semiempirical evaluation of the changes in mean square charge radii.[17]

First results of the measurements concerning the nuclear ground state spins of the investigated isotopes, experimental details involving a new variant of collinear laser spectroscopy used for the investigation, and $\delta\langle r^2\rangle$ values for the even isotopes were already reported in separate communications.[18,19] Here we present the complete set of hfs and IS results obtained during the study of Sr isotopes.

In Sec. II of this article, we give a brief description of the experimental procedure applied. The hfs and IS data are collected in Sec. III and the magnetic moments μ, the spectroscopic quadrupole moments Q_S, as well as the changes in mean square charge radii are derived from the data. These nuclear properties are discussed in Sec. IV with the main emphasis on the isotopic variations of $\langle r^2 \rangle$. For this purpose the $\delta\langle r^2 \rangle$ values are interpreted first in the framework of the Droplet model.[20] Quadrupole deformation effects in this model are evaluated with the help of experimental $B(E2)$ values. For Sr, $B(E2)$ values are available not only near the $N=50$ shell closure but also in the strongly deformed regions around $N=40$ and $N=60$.[21–25] This unique situation allows an extension of the discussion focusing on the influence of changes in the diffuseness of the nuclear charge distribution near the $N=50$ shell closure,[14] onto $\delta\langle r^2 \rangle$ values. Those aspects will mainly be discussed in a further interpretation of the experimental data in the framework of the Hartree-Fock (HF) plus BCS approach. We have calculated nuclear charge densities using the effective interaction SKa (Ref. 26) and the finite range force G0P (Ref. 27). The calculations are compared with the experimental results on quadrupole moments from $B(E2)$ values and changes in mean square charge radii evaluated from our IS measurements.

II. EXPERIMENT

The experiment was carried out on-line at the ISOLDE mass separator at CERN using the method of fast beam collinear laser spectroscopy. Hyperfine structure and isotope shift measurements on all isotopes with $78 \leq A \leq 98$ and on ^{100}Sr, including the isomers ^{83m,85m,87m}Sr, were performed in the $5s\,^2S_{1/2}-5p\,^2P_{3/2}$ ($\lambda=407.9$ nm) transition of the Sr ion (Sr II).

Two variants of the fast beam method were used for the measurements: one based on the optical detection on resonances (for $78 \leq A \leq 98$) and the other based on the counting of atoms produced in a state selective charge exchange process ($A=98$, $A=100$).[28] Details on the techniques and on their applications in on-line measurements of hfs and IS can be found in Refs. 29 and 30 and Ref. 19, respectively. The main features of the methods, as well as some details relevant for the present measurements are given below.

A. Isotope production

Neutron rich Sr isotopes were produced by fission of the uranium contained in a hot UC_2 target (65 g/cm^2) irradiated with the 600 MeV proton beam of the CERN synchrocyclotron. On the neutron deficient side, proton induced spallation in a Nb-powder target (50 g/cm^2) was used. Both target systems rely on a tungsten surface ionization source[31] for the production of singly charged Sr ions which are subsequently accelerated to energies of 60 keV. After mass separation the ion beam is guided to the experimental setup, where the fast beam serves as the sample for the laser spectroscopy measurements.

The beam intensities available for the measurements reached from 10^9 ions/sec for ^{88}Sr to 6×10^3 ions/sec for ^{100}Sr in the case of the UC_2 target and from 4×10^9 ions/sec for ^{86}Sr to 2×10^6 ions/sec for ^{78}Sr in the case of the Nb-powder target. The most short-lived isotope investigated was ^{100}Sr with a half-life of 214 (8) msec.

B. Fast beam laser spectroscopy

The measurement procedure based on the optical detection of resonance excitation follows closely that one described by Wendt *et al.* for the case of Ba^+ ions.[30] The ions are excited in an interaction region by the laser beam which is superimposed on the ion beam in collinear geometry. The resonance condition for excitation of the optical transition is

$$\nu_L = \nu_R \left[\frac{1-\beta}{1+\beta} \right]^{1/2} \tag{1}$$

with ν_L the laser frequency, ν_R the transition frequency, and $\beta=v/c$ the relative ion velocity, is achieved by Doppler turning, using a variable voltage applied to the interaction region. The fluorescence photons emitted by the excited ions are imaged onto a photomultiplier and detected with an overall efficiency of 5×10^{-3}.

All isotope shifts in Sr were measured relative to the stable isotope ^{88}Sr. Measuring cycles included, besides the reference isotope and the isotope under investigation, always a third isotope with a previously precisely measured isotope shift. This provides an on-line check for acceleration voltage drifts and other possible sources of systematic errors.

The principal experimental steps in the fast beam laser spectroscopy variant based on state selective neutralization are the following. Again, in collinear geometry, the ions are excited by the laser light but contrary to the optical case, the method exploits that the excited $5p\,^2P_{3/2}$ state decays partly into the low lying metastable $4d\,^2D_J$ states. This leads to a depopulation of the $5s^2S_{1/2}$ ground state. Through the state selectivity of the neutralization reaction in a sodium vapor, contained in a charge exchange cell installed downstream of the excitation region, this change in population is efficiently translated into a change in atomic charge state. A long interaction zone of 1.5 m for an efficient optical pumping is obtained by scanning the laser frequency instead of the ion velocity. The analysis of the charge state is achieved by electrostatically separating the remaining ions from the atoms and counting the secondary electrons emitted by impact of the atoms on an aluminum tape. For calibration of the laser frequency detuning, the laser is scanned across a fixed frequency range and the signal from a reference isotope (^{94}Sr) is observed optically at different ion velocities. In these scans the difference in the signal position is directly related to the difference in Doppler shift, thus establishing a frequency scale.

Figure 1 shows, as a typical example of the obtained spectra, the signals of ^{85}Sr and its isomer. These signals were recorded in a total measuring time of 2 min at a beam intensity of approximately 3×10^9 ions/sec. The observed linewidth is in the order of 40 MHz. It is mainly due to the natural linewidth in the investigated transition ($\Delta\nu_N=24$ MHz), a residual Doppler width

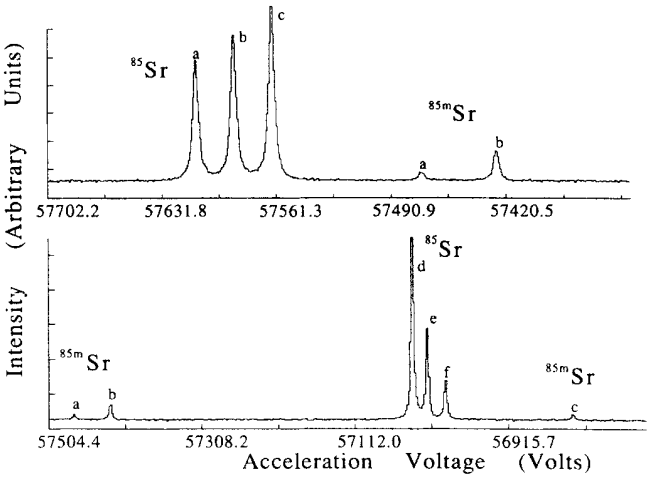

FIG. 1. Signal of ^{85}Sr and ^{85m}Sr representative for the $I=\frac{9}{2}$ isotopes below $N=50$ revealing $I=\frac{1}{2}$ isomeric states. The two graphs are from two separate measurements and they partially overlap. The hfs components for ^{85}Sr are labeled a–f and those of ^{85m}Sr a–c [$F(^2S_{1/2})\rightarrow F(^2P_{1/2})$]. For ^{85}Sr: a, 4→5; b, 4→4; c, 4→3; d, 5→6; e, 5→5; f, 5→4. For ^{85m}Sr: a, 1→1; b, 1→2; c, 0→1.

($\Delta\nu_D \approx 20$ MHz) caused by the energy spread of the Sr ions ($\Delta E \approx 2$ eV). With the optical detection scheme, the signal to noise ratios in the obtained spectra were larger than 15:1 for all investigated isotopes. The signal for ^{100}Sr, recorded by atom detection, exhibits a signal to noise ratio of 5:1. When compared to the photon counting technique, a sensitivity increase in the order of 2000 was achieved by the use of the nonoptical method. This is essentially due to the efficient counting of atoms, uninfluenced by scattered laser light which represents the major source of background in the optical detection scheme.

III. RESULTS

A. Data evaluation

For spectra of the even isotopes the IS with respect to ^{88}Sr is evaluated from

$$\delta\nu^{A,88}=\nu_R\left[\left[\frac{1-\beta^{88}}{1+\beta^{88}}\right]^{1/2}-\left[\frac{1-\beta^{A}}{1+\beta^{A}}\right]^{1/2}\right], \quad (2)$$

where ν_R is the transition frequency measured for naturally occurring Sr. The velocity v, corresponding to a particular resonance is evaluated from the precisely measured potential difference applied for accelerating the ions and from the experimental ground states masses tabulated in Ref. 32. For the investigated isomers, the known excitation energy[33] is taken into account in the calculations. In the case of spectra measured by nonoptical detection, the difference in channel position between the peaks of the reference isotope and the isotope of interest is translated to a difference in frequency using the MHz/channel scale established through the laser scan calibration described in Sec. II B. The frequency shift contains the IS and the Doppler shift which is easily calculated.

For the odd isotopes, Eq. (2) is used to evaluate the frequency difference between each hfs component and the reference isotope. Using this information, the magnetic dipole constant A and the electric quadrupole constant B can be evaluated from the expression[34]

$$W_F=\tfrac{1}{2}CA+B\frac{(3/4)C(C+1)-I(I+1)J(J+1)}{2I(2I-1)J(2J-1)}, \quad (3)$$

where W_F is the hfs energy of the sublevel with angular momentum F with respect to the center of gravity, and $C=F(F+1)-I(I+1)-J(J+1)$. As reported previously,[18] the spin I can be found simultaneously from Eq. (3). Together with the evaluation of the A and B factors, the hfs center of gravity is deduced from the positions of the hfs components. The IS of the odd isotopes is then given by the difference between the center of gravity and the ^{88}Sr reference.

The A and B factors, together with the spins are given in Table I. The IS data are tabulated in Table II. Their consistency can be checked through a King plot procedure[35] involving IS results obtained in other optical transitions. Figure 2 shows the King plot combining our

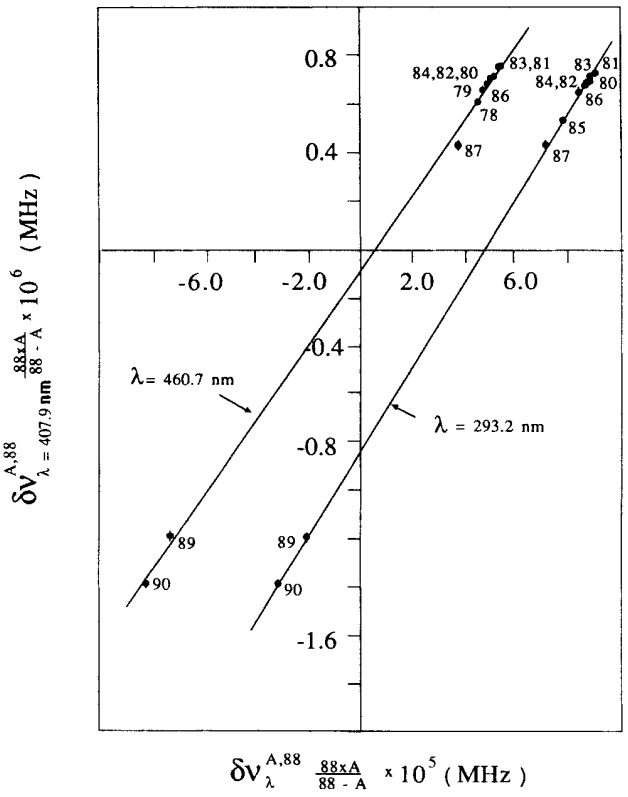

FIG. 2. King plot involving the isotope shifts in the ionic $\lambda=407.9$ nm transition and the atomic $\lambda=293.2$ nm (Ref. 13) and $\lambda=460.7$ (Refs. 14, 15, and 16) transitions, respectively.

TABLE I. Spins and hyperfine coupling constants of Sr isotopes (columns 2–5). The corresponding magnetic moments (μ) and spectroscopic quadrupole moments Q_S are given in columns 6 and 7, respectively. The error given for μ includes an estimate for the hfs anomaly (see text).

A	I	$A(^2P_{1/2})$ (MHz)	$A(^2P_{3/2})$ (MHz)	$B(^2P_{3/2})$ (MHz)	μ (μ_N)	Q_S (b)
79	$\frac{3}{2}$	1301.7(1.5)	−47.0(0.6)	191.9(1.7)	0.474(4)	0.726(62)
81	$\frac{1}{2}$	4477.6(3.5)	161.2(1.5)		0.543(4)	
83	$\frac{7}{2}$	975.4(0.9)	−35.1(0.3)	206.2(3.2)	0.829(2)	0.781(67)
83*m*	$\frac{1}{2}$	4786.4(7.7)	173.0(2.7)		0.581(4)	
85	$\frac{9}{2}$	915.2(0.7)	−32.9(0.3)	76.4(4.1)	1.000(2)	0.289(29)
85*m*	$\frac{1}{2}$	4943.7(6.3)	178.2(2.1)		0.600(4)	
87	$\frac{9}{2}$	1000.5(1.0)	−36.0(0.4)	88.5(5.4)	1.092 82(65)	0.335(20)
87*m*	$\frac{1}{2}$	5168.8(9.1)	185.7(4.2)		0.624(4)	
89	$\frac{5}{2}$	1890.4(1.1)	−68.3(0.4)	−73.4(2.4)	1.147(2)	−0.278(25)
91	$\frac{5}{2}$	1459.0(1.2)	−52.6(0.6)	12.3(3.0)	0.885(2)	0.047(12)
93	$\frac{5}{2}$	1306.2(1.2)	−47.2(0.6)	69.8(3.0)	0.793(2)	0.264(25)
95	$\frac{1}{2}$	4427.1(4.0)	−159.9(1.6)		0.537(2)	
97	$\frac{1}{2}$	4105.8(5.6)	−146.5(1.8)		0.498(2)	

measurements and those in the atomic $\lambda=460$ nm (Refs. 14 and 16) and $\lambda=226$ nm lines (Ref. 13), respectively. The straight line prediction of the King plot[35] is borne out in both cases. For the $\lambda=460$ nm line the ^{87}Sr shows some deviations already discussed in a previous comparison between the $\lambda=460$ nm and $\lambda=226$ nm data.[36]

TABLE II. Isotope shifts (column 2) and changes in mean square charge radii (column 3) of Sr isotopes relative to ^{88}Sr. For the $\delta\langle r^2\rangle$ values the experimental errors are given in parentheses. The errors given in the square brackets are due to the systematic uncertainties in the evaluation of $\delta\langle r^2\rangle$ from the isotope shift.

A	$IS^{88,A}$ (MHz)	$\delta\langle r^2\rangle^{88,A}$ (fm^2)
78	−893(12)	0.242(8)[41]
79	−865(10)	0.261(6)[37]
80	−782(11)	0.243(7)[33]
81	−710(9)	0.232(6)[28]
82	−574(10)	0.179(6)[24]
83	−495(6)	0.162(4)[20]
83*m*	−456(7)	0.134(4)[20]
84	−373(5)	0.116(3)[16]
85	−216(5)	0.048(3)[12]
85*m*	−259(5)	0.075(3)[12]
86	−171(3)	0.050(2)[8]
87	−56(3)	0.007(2)[4]
87*m*	−7(4)	0.024(3)[4]
89	−152(2)	0.124(1)[5]
90	−349(6)	0.277(4)[12]
91	−460(5)	0.374(3)[16]
92	−636(8)	0.512(5)[21]
93	−718(7)	0.590(4)[25]
94	−876(9)	0.715(6)[30]
95	−975(8)	0.802(5)[34]
96	−1198(10)	0.968(6)[40]
97	−1285(11)	1.047(7)[44]
98	−2166(11)	1.625(6)[59]
100	−2415(23)	1.832(15)[69]

B. Evaluation of spins and moments

We have previously reported on the evaluation of the nuclear ground state spins of Sr from the hfs data in the $5s\,^2S_{1/2}$ and $5p\,^2P_{3/2}$ states.[18] Their values are given in column 2 of Table I. In summary, the spins of ^{93}Sr and ^{97}Sr are revised to $I=\frac{5}{2}$ and $I=\frac{1}{2}$, respectively, while for the remaining isotopes the assignments from nuclear spectroscopy data are confirmed. Hyperfine structure measurements in the Sr II $5s\,^2S_{1/2}-5p\,^2P_{1/2}$ transition, which we have carried out more recently, again confirm the spin $I=\frac{1}{2}$ for ^{97}Sr.

The magnetic moments μ^x for all isotopes are related to the moment of the stable $I=\frac{9}{2}$ isotope ^{87}Sr by

$$\frac{A(^2S_{1/2})^x}{A(^2S_{1/2})^{87}}=\frac{I^{87}\mu^x}{I^x\mu^{87}}(1-\Delta^{x,87})\,, \tag{4}$$

where $\mu^{87}=-1.092\,82(65)\mu_N$ and $A(^2S_{1/2})^x$ and $A(^2S_{1/2})^{87}$ are the A factors of the $^2S_{1/2}$ state of the respective isotopes. $\Delta^{x,87}$ is the differential hyperfine anomaly, including the Breit-Rosenthal and Bohr-Weisskopf effect.[34] The above value for μ^{87} is based on an optical pumping result from Olschewski[37] and contains the diamagnetic correction from relativistic Hartree-Fock-Slater calculations by Feiock *et al.*[38]

The effects of the hfs anomaly are expected to be small. Experimental upper limits can be deduced from the ratios of the ground and excited state A factors $[A(^2S_{1/2})/A(^2P_{3/2})]$ which are constant throughout the entire series of isotopes.[18] As the ratios have much larger errors than the expected anomalies, we have used a semiempirical estimate of Moskowitz and Lombardi[39] combined with the estimate by Bohr and Weisskopf.[40] This leads to an additional uncertainty of $\approx 1\%$ in the values

of the magnetic moments, given in column 6 of Table I.

The spectroscopic quadrupole moments Q_S were evaluated from the ratio of the B factors using the moment of ^{87}Sr as a reference. The value $Q_S=0.335(20)$ b given by Heider and Brink[41] includes the Sternheimer shielding correction. The spectroscopic quadrupole moments are listed in column 7 of Table I.

A comparison of the moments with those obtained from hfs measurements by Anselment *et al.*[13] for the neutron deficient isotopes down to ^{81}Sr, shows excellent agreement, the only exception being $\mu(^{87m})$ where the authors quote $\mu^{87m}=+0.787(9)\mu_N$ compared to $\mu^{87m}=+0.627(2)\mu_N$ from our measurements. The value from our measurements is supported since (i) the 87*m* signal is simultaneously obtained with the signal of ^{87}Sr which also serves as the reference for the evaluation of μ^x for all other isotopes [see Eq. (4)], (ii) the hfs components from ^{87}Sr,^{87m}Sr are well resolved in the observed spectra which are very similar to those shown in Fig. 1, and (iii) the ratio of $A(^2S_{1/2})/A(^2P_{3/2})$ for ^{87m}Sr is consistent with those observed for the other isotopes (see Fig. 2 in Ref. 18).

C. Evaluation of changes in mean square charge radii

The IS between two isotopes with mass numbers A and A',$\delta\nu^{AA'}$ can be expressed as the sum of a mass shift $\delta\nu_m^{AA'}$ and a field shift $\delta\nu_f^{AA'}$.[17] The mass shift is represented as the sum of two terms, usually denoted as the normal mass shift $\delta\nu_n^{AA'}$ and specific mass shift $\delta\nu_s^{AA'}$:

$$\delta\nu^{AA'}=\delta\nu_n^{AA'}+\delta\nu_s^{AA'}+\delta\nu_f^{AA'}$$
$$=\frac{\nu_i}{1836}\frac{(A'-A)}{AA'}+\delta\nu_s^{AA'}+\delta\nu_f^{AA'}\,. \tag{5}$$

Here ν refers to the frequency of the investigated transition. The field shift is related to the change in charge distribution and is written as the product of the electronic field shift factor F and a power series of nuclear radial moments:

$$\delta\nu_f^{AA'}=F\sum_{k=1}^{\infty}\frac{c_k}{c_1}\delta\langle r^{2k}\rangle^{AA'}\,. \tag{6}$$

Neglecting moments higher than $\langle r^2\rangle$, which contribute in Sr roughly 2% to the sum in Eq. (6),[42] $\delta\langle r^2\rangle$ values are evaluated from the IS data with the help of Eqs. (5) and (6). The specific mass shift, which is not easily accessible through calculations,[17] as well as the calibration factor F, have to be known for this purpose.

For evaluating the mass shift and F, we follow along the lines indicated by Bender *et al.*[43] in a comprehensive analysis of atomic Sr isotope shifts in combination with muonic x-ray data for the isotope pairs $^{86-87}$Sr and $^{86-88}$Sr.[44] (i) We first evaluate the calibration factor F semiempirically using the Goudsmit-Fermi-Segre formula and the Fermi contact interaction in the $5s\,^2S_{1/2}$ state.[34] (ii) In a second step the mass and field shift in the $\lambda=407.9$ nm transition are separated through a King plot procedure[35] involving the muonic field shift data.

We have not directly used the $\delta\langle r^2\rangle$ values for the stable Sr isotopes given in Ref. 43 for calibration purposes since the alkalilike *ns-np* transition, investigated here, is considered to be most reliable for the semiempirical calculation of F. With the values for the muonic field shifts of $\delta E_\mu^{86-87}=-1115(100)$ eV and $dE_\mu^{86-88}=-1280(120)$ eV for the isotope pairs $^{86-87}$Sr and $^{86-88}$Sr, respectively, a specific mass shift $\delta\nu_s=-0.13(11)\delta\nu_n$ is found for the $\lambda=407.9$ nm transition.

A value close to zero for the specific mass shift in the investigated *ns-np* transition is supported by the empirical estimate of Heilig and Steudel[17] [$\delta\nu_s=0.3(9)\delta\nu_n$], by a parametrical analysis of level isotope shifts in Ref. 43 ($\delta\nu_s=0.14\delta\nu_n$) and by a comparison of isotope shift data with nuclear binding energies of Brechniac and Gerstenkorn[45] ($\delta\nu_s=0$).

The evaluation of the calibration factor F is carried out in detail in the Appendix. The result is

$$F^{86-88}=-1582(49)\ \text{MHz/fm}^2\,.$$

A relativistic Dirac-Fock (DF) calculation by Torbohm *et al.*[46] leads to $F_{\text{DF}}=-1174$ MHz/fm^2 revealing an often observed discrepancy, the calculated value of F being smaller by 20% to 30% than that found in the semiempirical analysis.

The changes in mean square charge radii derived from our IS measurements are given in column 3 of Table II. The errors quoted in parentheses are due to experimental uncertainties only. In the square brackets we quote the error arising in $\delta\langle r^2\rangle$ when $\delta\nu_s$ and F are altered by one error interval. A comparison of our $\delta\langle r^2\rangle$ values with those obtained by other authors in different atomic transitions[13,14,16] shows agreement within the limit of the errors arising from the calibration procedure. This underlines the agreement of the Sr data from different optical transitions, already demonstrated in Fig. 2, as well as the consistency of the evaluation of $\delta\nu_s$ and F in Sr I (Ref. 43) and the Sr II transition investigated in this work. [For the calibration of the IS in Ref. 13, a privately communicated set of muonic $\delta\langle r^2\rangle$ values was used. Taking these muonic $\delta\langle r^2\rangle^{88,86}=0.058(7)$ fm^2 and $\delta\langle r^2\rangle^{86,84}=0.085(7)$ fm^2 from Ref. 13 for the calibration of our IS data and still relying on the evaluated calibration factor F, a specific mass shift of $\delta\nu_s=+0.1\delta\nu_n$ is derived. This is consistent with the almost zero value we use.]

IV. DISCUSSION

A. Spins and moments

The moments of the investigated Sr isotopes and isomers shown in Fig. 3. A crude interpretation of the spins, the magnetic moments, and spectroscopic quadrupole moments can be obtained in a single particle approach. For this purpose we show in Fig. 4 the relevant neutron shell model states for this region of the nuclear chart as obtained from spherical mean field calculations described later in the text.

The ground state spin of the neutron rich $I=\frac{5}{2}$ isotopes has to be associated with the $2d_{5/2}$ neutron state. The systematics in the magnetic as well as in the spectro-

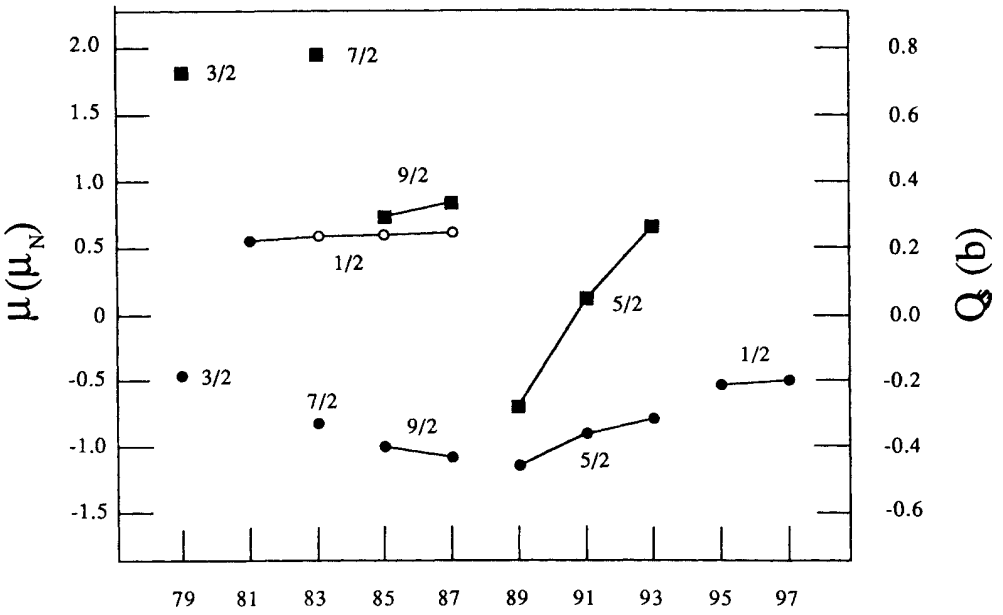

FIG. 3. Magnetic moments (solid circles) and spectroscopic quadrupole moments (squares) of the odd Sr isotopes and isomers between $A=79$ and $A=97$. The spin value of the respective isotope is indicated close to the data point. Successive isotopes (isomers) with the same spin are connected by solid lines. The magnetic moments of the $I=\frac{1}{2}$ isomers with $A=83$, 85, and 87 are represented by open circles.

scopic quadrupole moments support the single particle character of those isotopes. The magnetic moment of ^{89}Sr has been calculated by Nag and Pal.[47] Their calculations consider the core polarization correction to the extreme single particle (Schmidt) value, and also an exchange magnetic moment correction. The result of $-1.1839\mu_N$ is in close agreement with the observed $\mu(^{89}\text{Sr})=-1.147(2)\mu_N$ representing 0.6 times the Schmidt value for a $d_{5/2}$ neutron. A decreasing moment is observed for the subsequent members of the $d_{5/2}$ shell. The trend reflects the often observed increase of quenching of the Schmidt moments by core polarization, as expected from the increasing admixture of collective states. The spectroscopic quadrupole moments of the $I=\frac{5}{2}$ isotopes reveal a change in sign from negative to positive, with a moment close to zero for the midshell isotope (^{91}Sr). This is the behavior predicted from the single particle expression

$$Q_{\text{SP}}=\frac{2j-1}{2j+2}\langle r^2\rangle\frac{2j+1-2n}{2j-1}e\ , \tag{7}$$

where n is the occupation number in the $d_{5/2}$ subshell. The Q_{SP} for the single particle and single hole states are $Q_{\text{SP}}=\pm 0.1$ b, which is roughly 40% of the magnitude of the observed moments in ^{89}Sr and ^{93}Sr, respectively.

The very similar magnetic moments of the $I=\frac{1}{2}$ isotopes with mass $A=95$ and $A=97$ may be taken as an indication for their common origin in the $s_{1/2}$ shell model state which follows the $d_{5/2}$ level in sequence calculated in the HF approach (see Fig. 4). For $A=97$, the low spin value is favored due to the close level spacing between $3s_{1/2}$ and $1g_{7/2}$ and pairing in the higher j shell. The exceptionally small magnetic moments of those isotopes, which represent only 27% of the Schmidt value ($\mu_{\text{SP}}=-1.91\mu_N$), might be explained qualitatively by the mixing of the $s_{1/2}$ with the closely spaced $d_{3/2}$ and $g_{7/2}$ single particle states.

On the neutron deficient side the $1g_{9/2}$ and the $2p_{1/2}$ single particle states determine the spins and moments of most of the investigated isotopes and isomers. The magnetic moments of the $I=\frac{9}{2}$ isotopes ^{87}Sr and ^{85}Sr are 57% and 52%, respectively, of the Schmidt value for a single $g_{9/2}$ neutron. The trend of a decrease in quadrupole moment towards the middle of the shell is less pronounced than expected from the single particle ansatz of Eq. (7) which yields a ratio of $Q_{\text{SP}}(^{87}\text{Sr})/Q_{\text{SP}}(^{85}\text{Sr})=2$ in contrast to the observed ratio $Q_{\text{SP}}(^{87}\text{Sr})/Q_{\text{SP}}(^{85}\text{Sr})=1.1$. The $I=\frac{1}{2}$ isotope ^{81}Sr and the isomers with mass numbers $A=83$, $A=85$, and $A=87$ have magnetic moments only slightly below the Schmidt value for a $p_{1/2}$ neutron ($\mu_{\text{SP}}=0.638\mu_N$). This is expected since the $p_{1/2}$ shell is quite insensitive to core polarization, as well as mesonic contributions.[48] The revised $\mu(^{87m}\text{Sr})$ (see Sec. III B) fits well into the observed trend of nearly constant moments observed in the $p_{1/2}$ shell. The spin and the moments of the $I=\frac{7}{2}$ isotope ^{83}Sr were discussed extensively by Anselment *et al.*[13] who show that its ground state can be described as a $1(g_{9/2})^{-3}_{7/2}$ anomalous coupling state. For the $I=\frac{3}{2}$ isotope ^{79}Sr, the observed moments are consistent with the assignment of a $\frac{3}{2}^-$ [301] neutron orbital. Calculations of these moments performed by Heyde *et al.*[49] within the model of an odd particle coupled to the deformed even-even core, are in qualitative agreement with our experimental values of $\mu=0.474(4)\mu_N$ and

$Q_S = 0.726(62)$ b, respectively. For a comparison with the predictions for the intrinsic quadrupole moment (Q_0) by Möller and Nix,[50] $Q_0 = +3.55(27)$ b is derived from Q_S under the assumption of strong coupling. This is close to the calculated result of +3.2 b.

B. Changes of mean square charge radii

The changes of mean square charge radii of the investigated Sr isotopes are shown in Fig. 5. In this figure we have added the systematic $\delta\langle r^2\rangle$ data in the Sr neighbor Rb (Ref. 12) for comparison. Several common features in the gross behavior of the $\delta\langle r^2\rangle$ curves are expressed in both sets of data. A decreasing charge radius is observed as the neutron shell closure at $N=50$ is approached from the neutron deficient side. The shell closure is pronounced as a distinct kink in the $\delta\langle r^2\rangle$ curve. For the neutron rich isotopes, an almost linear increase is followed by a strong discontinuity at $N=59$–60.

The A dependence of the changes in mean square charge radii can be interpreted through a comparison of the data with model predictions. For this purpose, the Sr data are compared in the following to predictions from the macroscopic Droplet model,[20] as well as to results of calculations which we have carried out in a HF plus BCS approach.

1. Comparison with the droplet model prediction

In the Droplet model[20] the mean square charge radius of an isotope A is characterized to first order by (i) the proton sharp radius R_z, (ii) the quadrupole deformation of the charge distribution expressed by the deformation parameter α_2, which is the coefficient in an expansion of the nuclear shape by Legendre polynomials and, (iii) a diffuseness parameter b corresponding to the variance of a Gaussian folded into the sharp nuclear surface:

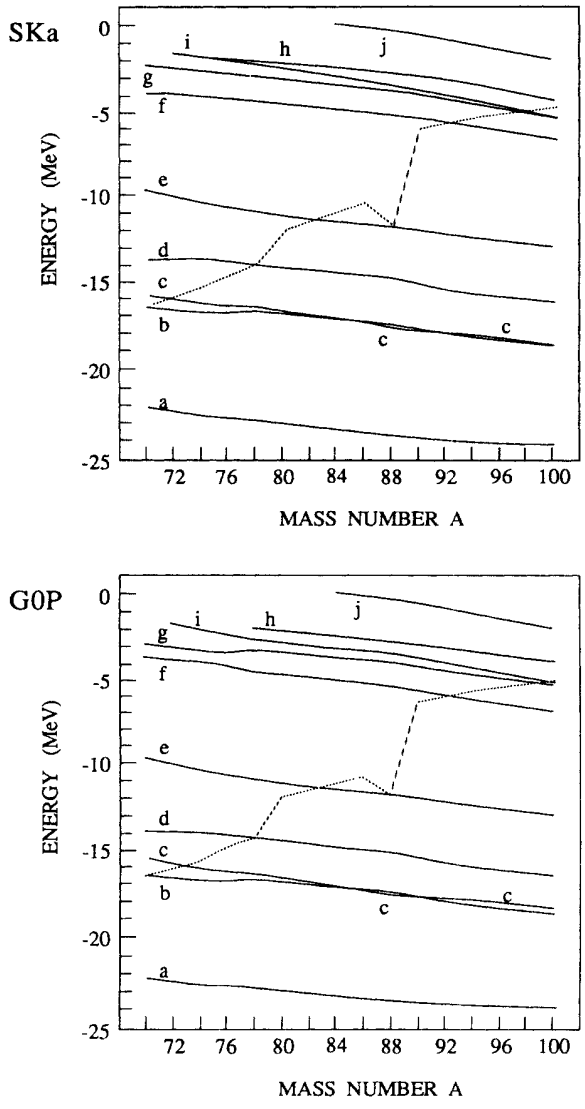

FIG. 4. Neutron energy levels obtained from spherical HF plus BCS calculations described in the text. The upper part displays the predictions of force SKa; the lower part those of force G0P. The dashed line represents the Fermi energy. The letters in the figure refer to the levels as follows: a, $1g_{9/2}$; b, $2p_{3/2}$; c, $1f_{5/2}$; d, $2p_{1/2}$; e, $1g_{9/2}$; f, $2d_{5/2}$; g, $3s_{1/2}$; h, $2d_{3/2}$; i, $1g_{7/2}$; j, $1h_{11/2}$.

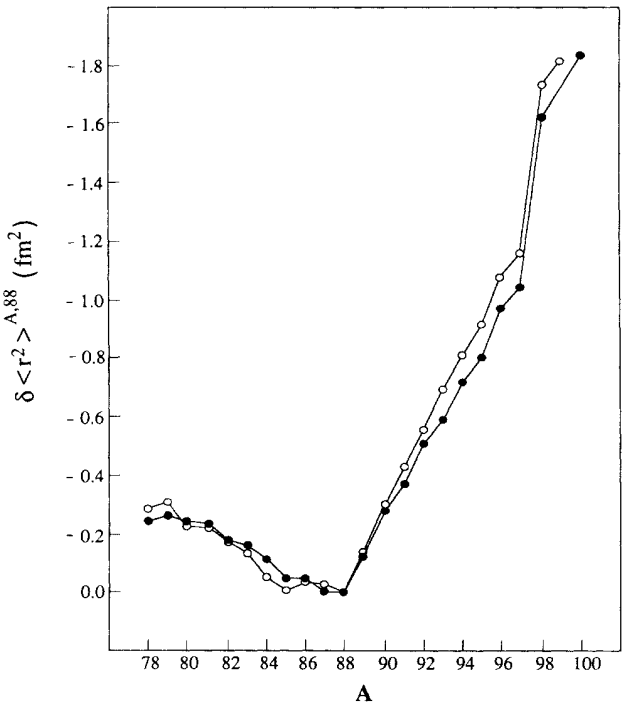

FIG. 5. Changes in mean square charge radii of Sr isotopes (solid circles). The data points are connected by a solid line to guide the eye. The results for Rb (Ref. 12) are added for comparison.

$$\langle r^2\rangle^A_{\rm DM}=\tfrac{3}{5}R_z^2(1+\langle\alpha_2^2\rangle+\tfrac{10}{21}\langle\alpha_2^3\rangle-\tfrac{27}{35}\langle\alpha_4^2\rangle)$$
$$+\tfrac{12}{175}C'R_z^2(1+\tfrac{14}{5}\langle\alpha_2^2\rangle+\tfrac{28}{15}\langle\alpha_2^3\rangle-\tfrac{29}{9}\langle\alpha_2^4\rangle)$$
$$+3b^2\ . \qquad (8)$$

The constant C' defined in Ref. 20 represents the Coulomb redistribution correction. Calculating the α_2 dependent proton sharp radius and, subsequently, $\langle r^2\rangle_{\rm DM}$ requires some information on the ground state deformation of the isotope considered. This information is commonly obtained for the even-even isotopes[6,51] by relating measurements of the reduced transition probabilities for $E2$ transitions connected with the 0^+ ground state $[B(E2;0^+\rightarrow 2_1^+)]$ to the nuclear quadrupole moment by

$$Q_0^2=\left[\frac{16\pi}{5}\right]B(E2;0^+\rightarrow 2_1^+)\ . \qquad (9)$$

The intrinsic quadrupole moment depends on α_2 through[20]

$$Q_0=\tfrac{6}{5}ZR_z^2(\alpha_2+\tfrac{4}{7}\alpha_2^2-\tfrac{1}{7}\alpha_2^3-\tfrac{94}{231}\alpha_2^4)$$
$$+\tfrac{48}{175}C'ZR_z^2(\alpha_2+\tfrac{6}{7}\alpha_2^2-\tfrac{4}{5}\alpha_2^3-\tfrac{1984}{1155}\alpha_2^4)\ . \qquad (10)$$

For the calculation of Q_0 we use the adopted $B(E2)$ values from Ref. 6 except for ^{98}Sr and ^{100}Sr where we evaluate the $B(E2)$ value from recent lifetime measurements of the first excited 2^+ state.[24,25]

No $B(E2)$ values are found in the literature for the neutron rich isotopes with $A=90$, 92, 94, and 96. However, a rough estimate of the $B(E2)$ values, and thus, of Q_0 and α_2 can be obtained from the energy of the first excited 2^+ level using the semiempirical relation[52]

$$B(E2,0^+\rightarrow 2_1^+)E_{2_1^+}=(12\pm4)Z^2A^{-1}\ (\mathrm{MeV}\,e^2b^2)\ . \qquad (11)$$

For a check of the validity of this relation in the Sr series, we have also calculated the $B(E2)$ values for the remaining isotopes with the help of Eq. (11). A comparison of the results (see column 3 of Table III) with the actually measured values shows reasonable agreement within the limits of error. The quadrupole moments calculated from the $B(E2)$ values are given in column 4 of Table III. From the quadrupole moments, the deformation parameter α_2 is calculated iteratively using Eq. (10) and the expression for the proton sharp radius given in Ref. 20. The standard Droplet model parameter set of Myers and Schmidt[20] is used in the calculation of R_Z.

In column 5 of Table III, we list the deformation parameters of the even-even Sr isotopes obtained from the $B(E2)$ values. Because of its more popular usage, we express the deformation by $\langle\beta_2^2\rangle^{1/2}$ where $\beta_2=(4\pi/5)\alpha_2$ is the coefficient in an expansion of the nuclear shape in spherical harmonics. The systematics in $\langle\beta_2^2\rangle^{1/2}$ based on the $B(E2)$ values, show a constant, moderate deformation for the heavy isotopes with $A\leq 96$. This behavior is commonly considered[7] to be the result of the stabilizing influence of the spherical shell gap, observed in the Nilsson single particle levels at $N=56$. A strong ground state deformation ($\beta_2\approx 0.4$) is reached for $A=98$ and $A=100$ in an abrupt way due to the reinforcement of the influence of the shell gaps at strong prolate deformation for $N=60$ and $Z=38$.[7] For the light isotopes around $N=38$, a similar high β_2 is observed. In contrast to the neutron rich isotopes the deformation in this region is reached in a continuous way.

Changes in mean square charge radii relative to ^{88}Sr, calculated from Eq. (8), with the use of the above deformation parameters and under the assumption of an isotopically independent surface parameter b,[20] are shown in Fig. 6 and compared to the experimental results. For the heaviest and lightest isotopes in the investigated series, the agreement between the experimental data and the droplet predictions is good. In the transitional regions between and below the $N=50$ shell closure, a systematic disagreement is observed.

The situation is similar to that one found in the neigh-

TABLE III. $B(E2)$ values for the even Sr isotopes from Refs. 6, 24, and 25 (second column) and calculated from the energy of the first excited 2^+ state (third column). The corresponding magnitude of the quadrupole moment $|Q|$ is given in the fourth column and the deformation parameter $\langle\beta_2^2\rangle^{1/2}$ in the fifth column.

A	$B(E2)$ (e^2b^2)	$B(E2)$ from E_{2^+} (e^2b^2)	$\lvert Q\rvert$ (b)	$\langle\beta_2^2\rangle^{1/2}$
78	1.07(13)	0.80(26)	3.28(21)	0.408(25)
80	0.84(7)	0.56(19)	2.90(13)	0.362(16)
82	0.513(20)	0.37(12)	2.272(44)	0.287(6)
84	0.28(4)	0.26(9)	1.68(12)	0.215(15)
86	0.106(16)	0.187(62)	1.03(8)	0.134(10)
88	0.092(5)	0.107(35)	0.962(26)	0.125(3)
90		0.232(77)	1.53(26)	0.192(30)
92		0.231(76)	1.53(26)	0.192(30)
94		0.220(73)	1.49(23)	0.185(31)
96		0.222(73)	1.49(23)	0.185(27)
98	1.31(6)	1.22(40)	3.63(8)	0.418(9)
100	1.45(8)	1.34(44)	3.82(10)	0.435(11)

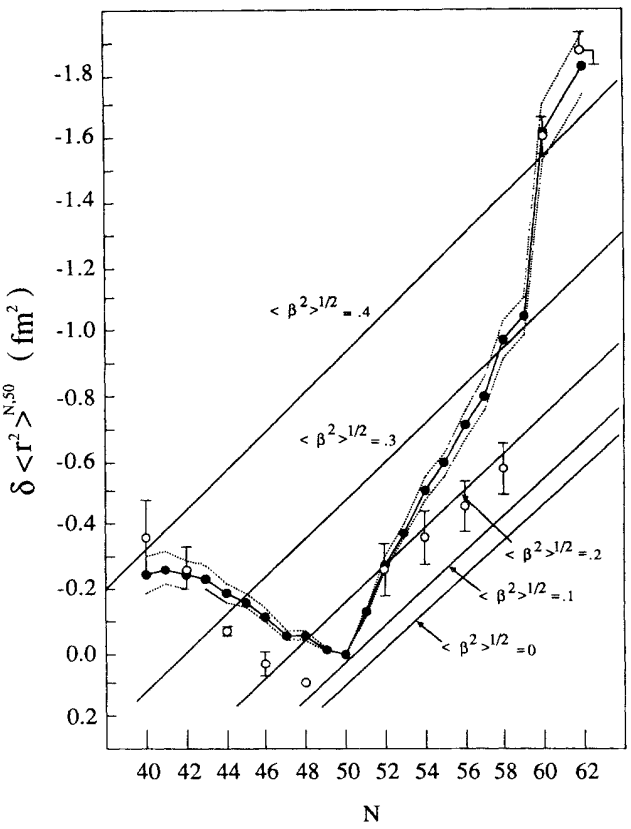

FIG. 6. Comparison between experimental changes in mean square charge radii (solid circles) and droplet model predictions corrected for quadrupole deformation calculated from $B(E2)$ values (open circles). The droplet model isodeformation curves are shown as solid lines. A value of $\langle\beta^2\rangle^{1/2}=0.125$ for ^{88}Sr was used as the reference. The dashed lines indicate the systematic errors for the $\delta\langle r^2\rangle$ values from the calibration procedure.

boring odd-Z element Rb (Ref. 12) where, apart from details, the general trends of the present $\delta\langle r^2\rangle$ curve in Sr agree rather well. In a theoretical study of the influence of collective zero-point motion on the development of the Rb mean square charge radii,[5] it was concluded that theoretical values for the collective width $\langle\beta^2\rangle$ fail to explain the sharp change in the slope of the $\delta\langle r^2\rangle$ curve.

For the neutron deficient isotopes, possible reasons for the disagreement have been discussed[14] in connection with HF plus BCS calculations based on the forces SKa and G0P. The importance of a nonconstant diffuseness parameter in the droplet expression for $\langle r^2\rangle$ [see Eq. (8)] has been pointed out. We have extended those calculations from the previously considered mass range between $A=84$ and $A=90$ to isotopes further away from stability in order to get more insight into the possibility of a microscopic model description of the changes in mean square charge radii.

2. *HF plus BCS calculations*

The calculations were carried out in the HF plus BCS approach using the effective force SKa,[26] and the finite range interaction G0P.[27] They closely follow those described in Refs. 14, 53, and 54, and we restrict ourselves to the presentation of the results which are relevant for the interpretation of the IS data in the investigated Sr series. These results are collected in Table IV. The HF plus BCS energies of the very deformed prolate states were corrected using the cranking approximation for the moment of inertia of the nucleus and the mean value of the square of the angular momentum ($\langle J^2\rangle$).[55,56] This correction, which provides on the average a gain in binding of 2.3 MeV, corresponds to a perturbative angular momentum projection of the deformed wave function into the 0^+ state.[57,58]

Both forces predict that ^{80,82,84,86}Sr and ^{90,92,94}Sr are nuclei soft against deformation. The softness, or the width of the energy plateau around $Q_0=0$, increases as one increasingly departs from the shell closure at $N=50$. Force SKa indicates that ^{76}Sr should be the first rigidly deformed neutron deficient isotope. However, no prolate nuclear shape is obtained with force G0P in this mass region and a slightly oblate deformation is predicted for ^{76}Sr.

For the neutron rich isotopes ^{96,98,100}Sr, force SKa indicates strong prolate deformation ($Q_0\approx 4.0$ b). For each of these nuclei, the axial symmetric calculation provides another minimum in the oblate region. The binding energy differences between the lowest oblate and prolate minima range between 2 (^{96}Sr) and 4 MeV (^{100}Sr). Force G0P also indicates prolate and oblate minima for the above isotopes. The energy differences between minima are, however, considerably smaller for this interaction. They are in the range of a fraction of a MeV, the minimum on the oblate side around $Q_0=-1.2$ b being the lower.

The disagreement in the results for the lightest and heaviest investigated isotopes using these two interactions is surprising since the single particle eigenvalues for spherical nuclei show a remarkable coincidence (see Fig. 4). A careful analysis shows that the same also holds for equally strong prolate deformation. The result is that shell structure effects may be ruled out as the cause for the differences in the shapes of the lowest energy solutions. The disagreement rather points to differences in the forces' macroscopic properties, in particular, in the surface and surface-symmetry energies.

For force SKa, the result of close to zero deformation in the transitional nuclei and of large prolate deformation for the isotopes far off stability is in qualitative agreement with the findings of other authors using Strutinsky type[10,49,50,59] or mean field approaches.[1,60] The experimental moments for $A=98$ and $A=100$ of $Q_0\approx 3.7$ b derived from the $B(E2)$ values (see Table III) are reproduced. On the neutron deficient side, the predicted sphericity of the lightest nuclei is at variance with the experimental findings. This is further discussed in Sec. IV B 2 b.

(*a*) *Changes in mean square charge radii.* Changes in mean square charge radii are determined as in Refs. 14, 54, and 61 by adding the following corrections to the HF plus BCS proton mean square radii: (i) a proton and neutron form factor correction, (ii) a correction due to the spurious center of mass motion, and (iii) an electromagnetic spin orbit correction. The mean square proton

($\langle r^2\rangle_p$) and the corrected charge ($\langle r^2\rangle_c$) radii are given in Table IV. For the isotopes between $A=78$ and $A=94$, where the spherical binding energy minimum was found to be the absolute one or less than 1 MeV above the absolute minimum, the $\langle r^2\rangle$ corresponding to the spherical solution is given. A comparison of $\delta\langle r^2\rangle_p$ and $\delta\langle r^2\rangle_c$ shows a sizable contribution to $\delta\langle r^2\rangle$ from the above corrections when the $1g_{9/2}$ shell is filled on the neutron deficient side. No relevant net effect on $\delta\langle r^2\rangle_c$ is observed in the neutron rich region.

The comparison of the predicted $\delta\langle r^2\rangle_c$ values with the experimental ones (see Fig. 7) show that the calculations using force SKa give a good description of the gross behavior of the data. The shell effect at $N=50$ is pronounced. On the neutron rich side, the transition from spherical to strongly deformed shape, which is indicated in the systematics of the calculated quadrupole moments (see Table IV), reproduces qualitatively the observed discontinuity in the $\delta\langle r^2\rangle$ curve. The suddenness of this transition is underlined, however, the onset of deformation appears two neutron numbers too early. For force G0P, the shortcomings concerning the shape transition in the neutron rich region (see above), are also displayed in the curve of $\delta\langle r^2\rangle$ values and we restrict ourselves for a further discussion to the results from force SKa only.

The predictions for the isotopes between $A=78$ and $A=94$ represent the changes in mean square charge radii at spherical shape. In this region, the difference between the calculated $\delta\langle r^2\rangle_c$ values and the experimental ones may be attributed mainly to dynamical contributions to the ground state deformation, which are suggested by the ratios of the energies of the first excited 4^+ to the first excited 2^+ states.[62] Those ratios reach from a value expected for a good vibrator of $E_{4^+}/E_{2^+}=2.0$ (^{90}Sr, ^{86}Sr) to $E_{4^+}/E_{2^+}=2.2$ on the neutron rich side (^{96}Sr) and $E_{4^+}/E_{2^+}=2.81$ for ^{78}Sr on the neutron deficient side.

In order to obtain a crude verification of this vibrational description in the region where spherical shape is predicted, we include quadrupole deformation effects into the HF calculations in an empirical way[60] by calculating $\delta\langle r^2\rangle_c$ values from the Droplet ansatz of Eq. (8) with

TABLE IV. Summary of the HF plus BCS calculations with forces SKa and G0P for the Sr series between $A=76$ and $A=100$. The second column shows the binding energy per nucleon. In the third and fourth columns the proton and neutron pairing gaps are listed. The quadrupole moment is shown in the fifth column and the proton and charge mean square radii in column six and seven, respectively. The surface width b_c and central charge radius C_c corresponding to the spherically constrained solution in the HF calculations is shown in the last two columns.

A	E/A (MeV)	Δp (MeV)	Δn (MeV)	Q (b)	$\langle r^2\rangle_p$ (fm^2)	$\langle r^2\rangle_c$ (fm^2)	b_c (fm)	C_c (fm)
				SKa				
76	−8.334			+3.84	18.095	18.516	1.000	4.732
78	−8.428	1.014		0	17.134	17.568	1.001	4.751
80	−8.512	0.959	1.222	0	17.185	17.594	0.991	4.765
82	−8.578	0.904	1.339	0	17.243	17.631	0.982	4.779
84	−8.632	0.848	1.253	0	17.305	17.668	0.974	4.794
86	−8.681	0.797	1.144	0	17.374	17.714	0.966	4.809
88	−8.716	0.752		0	17.438	17.755	0.959	4.823
90	−8.665	0.770	1.138	0	17.580	17.888	0.961	4.846
92	−8.606	0.652	1.390	0	17.715	18.019	0.963	4.867
94	−8.551	0.870	1.515	0	17.870	18.170	0.965	4.893
96	−8.511		0.793	+4.48	19.600	19.944	0.962	4.930
98	−8.455			+3.99	19.485	19.807	0.961	4.960
100	−8.388		0.400	+3.99	19.600	19.916	0.961	4.995
				G0P				
76	−8.124			−1.45	17.429	17.850	1.023	4.744
78	−8.228	0.929		0	17.606	18.034	1.018	4.780
80	−8.312	0.835	1.243	0	17.608	18.011	1.004	4.790
82	−8.379	0.754	1.351	0	17.621	18.003	0.991	4.805
84	−8.442	0.673	1.453	0	17.633	17.993	0.978	4.818
86	−8.486	0.588	1.143	0	17.670	18.008	0.966	4.835
88	−8.515	0.519		0	17.686	18.002	0.956	4.844
90	−8.503	0.579	1.172	0	17.814	18.123	0.956	4.871
92	−8.473	0.401	1.442	0	17.991	18.292	0.954	4.913
94	−8.439	0.749	1.562	0	18.132	18.428	0.954	4.492
96	−8.400			0	18.278	18.575	0.953	4.972
98	−8.370			−1.15	18.564	18.870	0.950	5.001
100	−8.319			−1.15	18.735	19.045	0.947	5.032

$\langle r^2\rangle = \frac{3}{5}R_z^2$ taken from the HF calculations and α_2^2 evaluated from the $B(E2)$ values (see Table III). Since the HF calculations take care automatically of Coulomb redistribution effects and of variations in the surface region of the charge distribution, only the first term on the right-hand side of Eq. (8) enters.

The HF values corrected for α_2 are shown in Fig. 8. The agreement with the experimental values in the mass range between $A=82$ and $A=94$ is good, thus improving the systematic deviations between experiment and the Droplet predictions in this region (see Sec. IV B 1). On the other hand, the agreement is very poor for the lightest isotopes with $A=78$ and $A=80$. Alternatively, we have calculated in the HF plus BCS approach the change in mean square charge radius between ^{88}Sr and ^{78}Sr assuming a rigid nuclear density deformation $\beta_2=0.42$ for ^{78}Sr. For those calculations, besides force SKa, we have also used the Skyrme interactions S III and S VI, used by Bonche *et al.*[1] and Campi and Epherre,[60] respectively, for systematic investigations of nuclear properties in the Zr region. The results are included in Fig. 8. The comparison with the present experiment shows that the experimentally observed $\delta\langle r^2\rangle^{78,88}=-0.25$ fm^2 is overestimated by a factor varying between 2 and 4.4, depending on the specific force. The systematic overestimation of the $\delta\langle r^2\rangle_c^{78,88}$ by all forces, as well as by the deformation corrected spherical SKa results, suggests an unusual shape sharing structure for this isotope (and probably for ^{80}Sr) with a different mean value for the deformation of the 2^+ than the 0^+ ground state. This hypothesis is supported by the apparent lack of shape rigidity in the rotational ground state band.[23] Despite the large $B(E2)$ value, ^{78}Sr shows a $E_{4^+}/E_{2^+}=2.81$, which is atypical for a rigid rotor and, furthermore, an increase in the moment of inertia with spin. Only at $I\geq 10$ is the rigid shape approached, while it is established in its odd-A neighbors ^{77}Sr and ^{79}Sr already at low spin.

Coming back to the $N=50$ shell closure, the slope change observed in the curve of the calculated $\delta\langle r^2\rangle_c$ values and the good description of the experimental values between $A=82$ and $A=94$ after inclusion of zero-point quadrupole vibrations indicates that the shell effect is only partially caused by deformation effects. In order to study the shell closure in more detail, we give, in the following, the results of a deeper analysis of the HF calculations.

(*b*) *The proton-neutron interaction near* $N=50$. Analysis of the microscopic (spherical constrained) calculations, concerning the shell effect at $N=50$, shows that

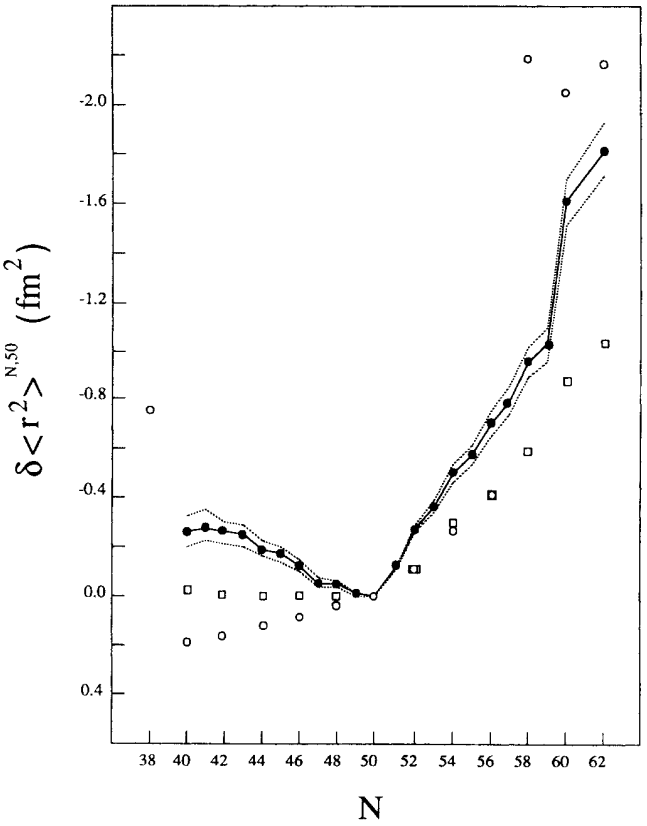

FIG. 7. Comparison of the experimental $\delta\langle r^2\rangle$ values (solid circles) with the results from HF plus BCS calculations. The dashed error band indicates the uncertainty in the $\delta\langle r^2\rangle$ values due to the calibration procedure. The predictions from force SKa are shown as open circles; those from G0P as open quadrangles.

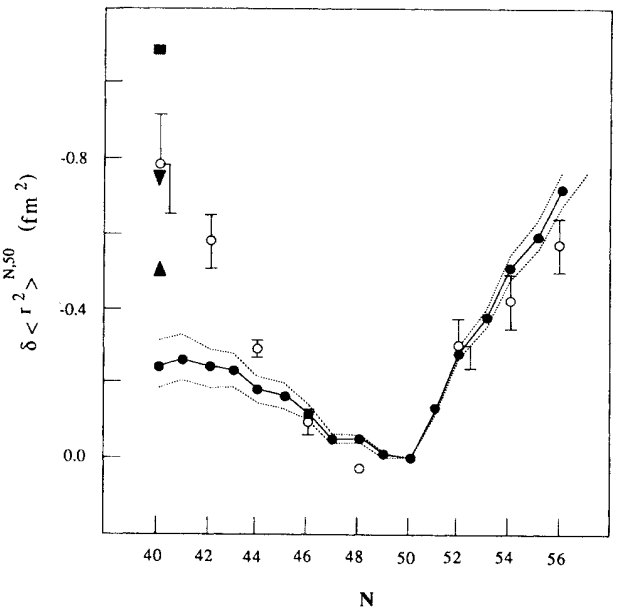

FIG. 8. Comparison between experimental $\delta\langle r^2\rangle$ values (solid circles connected by a solid line) and the results from the HF calculations using force SKa, for Sr isotopes in the region of predicted spherical shapes. The theoretical $\delta\langle r^2\rangle$ values are corrected for deformation using experimental $B(E2)$ values as described in the text. For $N=40$, the results of HF calculations with different interactions are shown for the case when a rigidly deformed nuclear charge distribution with $\beta=0.42$ is assumed. The quadrangle represents the result for force SKa; the triangle that for force Sr III and the inverted triangle that for force S VI.

the slope of the change in mean square charge radii is larger when the neutron chemical potential [Fermi energy $E_f(\nu)$] is closer to orbitals with n radial nodes than to those with $n-1$ radial nodes (see Fig. 4). The overall structure of the $\delta\langle r^2\rangle$ curve is produced by the proton-neutron interaction. Only the monopole part of the interaction plays a role in the spherically constrained calculations, i.e., only the radial dependence of the wave function is important in the matrix element of the proton-neutron force. The wave function in our calculations is of the quasiparticle type, i.e., takes into account the monopole pairing correlations in the $T_Z=1$ channel, which smooths out the occupation of the neutron orbitals n,l,j (n: number of nodes in the radial direction; l: orbital quantum number; $j=l\pm\frac{1}{2}$: angular momentum corresponding to the spin orbit coupling) in an energy region $E_f(\nu)\pm 10$ MeV.

Our results suggest that in a delicate balance the change in polarization of the proton orbitals closer to the Fermi surface due to the addition of two neutrons is going to dominate the stretching of the nuclear mean square radius. In the case of Sr, the three most external orbitals have $n=1$ $(1f_{5/2})$ and $n=2$ $(2p_{1/2})$ and $(2p_{3/2})$, but to a lesser extent $n=1$ $(1f_{5/2})$ for the heaviest nuclei. Using oscillator wave functions and a two body contact interaction,[63] one finds that a larger overlap between neutron and proton wave functions is favored when both wave functions have $n=1$. This result, when extended to $n=2$ and $n=3$, once more showed that the energy matrix elements are more attractive when the node numbers for proton and neutron wave functions are equal. Furthermore, self-consistent calculations show that for those orbitals belonging to the same principal oscillator quantum number with $E_F(\nu)\leq -5$ MeV, the wave function with n radial nodes are more extended in the radial direction than those with $n-1$ radial nodes.

A consequence of the above results is that if for the Sr series two neutrons are added. (i) Below $N=50$, mainly into the orbital $\nu(1g_{9/2})$, this orbital couples more to the $\pi(1f_{5/2})$ than to the $\pi(2p_{3/2})$ and $\pi(1p_{1/2})$ orbitals and the change in mean square charge radii is relatively flat over this region. (ii) Above $N=50$, mainly into the orbital $\nu(2d_{5/2})$, this orbital couples more to the $\pi(2p_{3/2})$ and $\pi(2p_{1/2})$ orbitals than to the $\pi(1f_{5/2})$ state and we find a large change in slope with a rapid increase of $\langle r^2\rangle$ for the neutron rich isotopes, thus pronouncing the shell closure.

The effects of the neutron-proton interaction on the properties of the density distribution can be studied in detail. We investigate here the influence on the external region of the charge distribution, to which, by definition, the mean square charge radii are most sensitive. For this discussion, we introduce the leptodermous parameters (i) C_c which is the distance from the center of the nucleus to the point of the maximum slope in the charge density and (ii) b_c, the symmetrical surface width defined by

$$b_c=\left[\int_{C_c}^{\infty}\rho_c(r)(r-C_c)^2dr\Big/\int_{C_c}^{\infty}\rho_c(r)dr\right]^{1/2}. \quad (12)$$

This parametrization allows a model-independent interpretation of the HF plus BCS densities, in the sense that no arbitrary function is used to fit the calculated charge distribution. Contributions to the mean square charge radii from charge asymmetries and from shell effects in the core region are neglected in this approximation.[64,65] A linear connection between b_c and the surface width parameter b, used before in the discussion of the data in the frame of the Droplet model, can be established for the mass region considered here.[14]

Figure 9 shows the parameters C_c and b_c evaluated from the HF plus BCS results. C_c shows a steady but not constant increase over the entire mass range. Starting from the $N=50$ shell closure, the surface width shows an almost linear increase of 4% towards the neutron deficient isotopes and only small variations for the isotopes beyond $N=50$.

In the frame of HF+BCS calculations, the decrease of b_c combined with a relatively low rate of increase of C_c in going from ^{78}Sr to ^{88}Sr, leads to the small predicted variation of $\delta\langle r^2\rangle$ with a slope of only 0.04 fm^2/2N. An increase in the slope of C_c above $N=50$ at nearly constant b_c results in the larger variation of $\langle r^2\rangle$ on the neutron rich side. The overall structure of the b_c curve is surprisingly similar to that one found in the proton surface widths in an isobaric series.[65] In this case, it was shown that when the Coulomb force is turned off, the proton width shows minor changes ($\approx 3\%$) with the asymmetry $I=(N-Z)/A$, whereas the Coulomb force is responsible for changes as high as 7% toward proton rich nuclei, its

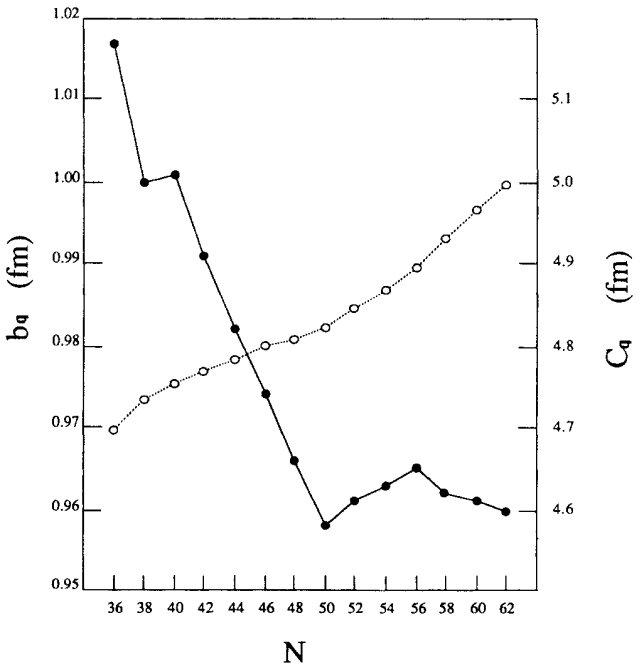

FIG. 9. Charge surface width parameter b_c (solid circles) and central charge radius C_c (open circles) for Sr isotopes as obtained from spherically constrained HF calculations using force SKa.

effect decreasing toward neutron rich nuclei. Calculations with force SKa with and without Coulomb interaction show that for $A=78$ the Coulomb force is responsible for a 4% larger charge surface diffuseness. This is helpful to reduce to some extent the unusual ratio of the repulsive Coulomb energy to binding energy for this proton rich nucleus. This high ratio decreases with increasing neutron number also reducing the effect of the Coulomb interaction on the leptodermous parameters.

V. SUMMARY AND CONCLUSIONS

Hyperfine structures and isotope shifts in the strontium isotopes between $A=78$ and $A=100$ were measured by fast-beam collinear laser spectroscopy. Nuclear spins, moments, and changes in mean square charge radii were extracted from the data.

The spins and moments of the odd isotopes and isomers between $A=81$ and $A=97$ were discussed qualitatively in the single particle model which explains the gross features of the spins and moments observed. The isotope ^{79}Sr reveals a well deformed prolate ground state characterized by the $\frac{3}{2}^-$ [301] neutron orbital. A quantitative interpretation of the data in a more elaborate model is desirable. Calculations in the Lund particle rotor model are currently being carried out and will be presented at a later time.

The changes in mean square charge radii were interpreted in the framework of the Droplet model corrected for quadrupole deformation with the help of $B(E2)$ values and with the help of HF plus BCS calculations. In a consistent picture the changes of the charge radii of the heaviest isotopes with $A=98$ and $A=100$ can be attributed to quadrupole deformation effects. For the remaining isotopes, the situation is more complex.

For the isotopes between $A=82$ and $A=96$, a systematic discrepancy is observed between the Droplet predictions and the experimental $\delta\langle r^2\rangle$ values. This discrepancy is removed in the HF plus BCS calculations for most of the isotopes in this region due to a more pronounced shell effect at spherical shape. The different slopes for the isotopes with $N<50$ and $N>50$, respectively, were shown to be the result of the different manifestations of the neutron-proton interaction mainly involving the nucleons in the $1g_{9/2}$ and $2d_{5/2}$ neutron and $1f_{5/2}$, $2p_{3/2}$, and $2p_{1/2}$ proton states. In a macroscopic picture, this interaction manifests itself through a steady increase of the central radius of the charge distribution with increasing neutron numbers. Simultaneously, a decrease in the surface width of the charge distribution is observed for the neutron deficient isotopes and an almost constant width for the neutron rich isotopes. The magnitude of the changes in surface width found in the HF calculations is less than 1% per two neutrons. The sensitivity of the changes of the mean square charge radii to small variations in the surface part of the charge distribution indicates that in general not all deviations of the experimental $\delta\langle r^2\rangle$ values from the spherical predictions of macroscopic models, such as the Droplet model, can safely be attributed to deformation effects.

For the lightest investigated isotopes ^{78}Sr and ^{80}Sr, for which measurements of the $B(E2)$ values indicate strong ground state deformation, no satisfactory description of the changes in mean square charge radii is obtained in the HF plus BCS approach. For ^{78}Sr, the results from spherical calculations corrected for quadrupole deformation, as well as deformed calculations with the interactions SKa, S III, and S VI yield systematically higher $\delta\langle r^2\rangle$ values than those observed experimentally. The results suggest a shape-sharing structure for ^{78}Sr and also possibly ^{80}Sr, with different mean values for the deformations of the ground and the first excited 2^+ state leading to an overestimation of the ground state quadrupole deformation when extracted from $B(E2)$ values. In this light, the good droplet model description for the lightest isotopes seems to be fortuitous. For a better test of the microscopic model an extension of the measurements to ^{76}Sr, which is predicted to be the first rigidly deformed neutron deficient isotope, is desirable. Recent attempts to investigate this isotope show that a measurement is out of the reach of our presently applied technique considering the yields available at the ISOLDE mass separator.

ACKNOWLEDGMENTS

We would like to thank Dr. N. DeTakacsy for helpful discussions and Dr. N. Koller and Dr. L. Zamick for the support given to one of us (D.B.) during parts of this work. This work was supported by the Belgian Interuniversity Institute for Nuclear Science (IIKW), the Canadian Natural Science and Engineering Research Council (NSERC), and the German Federal Minister for Research and Technology (BMFT) under Contract No. 06MZ4581. One of us (R.E.S.) is a research associate of the Belgian Foundation for Scientific Research (NFWO).

APPENDIX: EVALUATION OF THE ELECTRONIC FIELD SHIFT FACTOR F IN THE $5s\ ^2S_{1/2}-5p\ ^2P_{3/2}$ TRANSITION OF Sr II

Following the notation of Heilig and Steudel,[17] the calibration factor F can be expressed as

$$F=\pi a_0^3\Delta|\Psi_0|^2_{5s-5p}f_{(Z)}/Z\ . \tag{A1}$$

Here $\Delta|\Psi_0|^2_{5s-5p}$ represents the nonrelativistic change of the electron charge density at the point nucleus during the optical transition and $f_{(Z)}$ is a relativistic correction factor also taking account of the finite nuclear charge distribution. For the isotope ^{88}Sr-^{86}Sr, $f_{(Z)}$ is calculated[17] with a theoretical isotope shift constant $C^{86-88}_{\text{unif.}}$ from Ref. 43:

$$f^{86-88}_{(Z)}=3271\ \text{MHz/fm}^2\ . \tag{A2}$$

The change of the electron charge density may be written for the investigated *ns-np* transition as

$$\Delta|\Psi_0|^2_{5s-5p}=\beta|\Psi^2|_{5s}\ , \tag{A3}$$

where β is the screening factor and $|\Psi_0|^2_{5s}$ the charge density of the electron in the $5s$ ground state. Dirac-Fock calculations by Torbohm *et al.*[46] yield $\beta=1.11$. For finding $|\Psi_0|^2_{5s}$ the Goudsmit-Fermi Segre (GFS) formula as well and the hyperfine splitting of the $^2S_{1/2}$ state can be used.[34]

In the GFS approach, $|\psi_0|^2_{5s}$ is related to the quantum defect σ by

$$|\Psi_0|_{5s}a_0^3=\frac{Z_iZ_a^2}{\pi(n-\sigma)}\left[1-\frac{d\sigma}{dn}\right] . \quad \text{(A4)}$$

where $Z_i=Z=38$ and $Z_a=2$. With the Rydberg-Ritz relation one obtains $(n\text{-}\sigma)=Z_a\sqrt{R_\infty/T}=2.221$ and for the second term on the right-hand side of Eq. (A4)

$$d\sigma/dn=(d\sigma/dT)/[d\sigma/dT-(n-\sigma)/2T]=-0.081 .$$

Since for the *ns* states the variation of σ with the term values is not constant as expected for an unperturbed series, $d\sigma/dT$ was found through a second order polynomial fit to σ. The GFS relation leads to

$$|\Psi_0|^2_{5s}=4.772a_0^{-3} . \quad \text{(A5)}$$

Expressed by the hyperfine splitting of ^{87}Sr, $\Delta|\Psi_0|^2_{5s}$ becomes

$$|\Psi_0|^2_{5s}a_0^{-3}=\frac{3}{8}\frac{1836.1\,a_s^{87}I^{87}}{R_\infty\alpha^2\pi a_0^3F_r(Z)(1-\delta)(1-\epsilon)\mu_I^{87}} . \quad \text{(A6)}$$

The relativistic correction $F_r(38)=1.597$, the Breit Rosenthal correction $(1-\delta)=0.992$, and the Bohr-Weisskopf correction $(1-\epsilon)=0.999$ are taken from Ref. 43. Our hfs measurements in this $I=\frac{9}{2}$ isotope give $a_s^{87}=-1000.5(8)$ MHz which together with a magnetic moment of $\mu_I=-1.092\,82\mu_N$ (Ref. 37) leads to

$$|\Psi_0|^2_{5s}=4.485a_0^{-3} ,$$

in good agreement with the value found from the GFS formula. Taking the average of Eqs. (A5) and (A7), results in a calibration factor

$$F^{86,88}=-1582(49)\ \text{MHz/fm}^2 ,$$

where the error takes into account the variation of $|\Psi_0|^2_{5s}$ found through the two different approaches described above.

*Present address: Department of Radiation Oncology, State University of New York at Stony Brook, Stony Brook, NY.
†Present address: Goddard Space Flight Center (NASA), Greenbelt, MD.
‡Present address: Physikalisch Technische Bundesanstalt, Berlin 1, Federal Republic of Germany.

[1]P. Bonche, H. Flocard, P. H. Heenen, S. J. Krieger, and M. S. Weiss, Nucl. Phys. **A443**, 39 (1985), and references therein.
[2]D. P. Analpara, K. H. Batt, and A. Abouzi, Nucl. Phys. **A445**, 1 (1985).
[3]D. Galeriu, D. Bucurescu, and M. Ivascu, J. Phys. G **12**, 329 (1986).
[4]J. Eberth, M. Wiosna, T. Milaeus, N. Schmal, S. Skoda, J. Busch, W. Teichert, P. v. Brentano, J. H. Hamilton, A. Ramayya, X. Zhao, C. F. Maguire, W. C. Ma, T. M. Cormier, M. Satteson, J. D. Cole, R. B. Piercy, M. A. Herath-Banda, E. F. Zganjar, M. O. Kortelahti, G. A. Leander, and W. Nazarewicz, in *Proceedings of the Fifth International Conference on Nuclei Far From Stability (Roseau Lake, 1988)*, AIP Conf. Proc. No. 164 (AIP, New York, 1989), p. 268.
[5]W. D. Myers and P. Rozmej, Nucl. Phys. **A470**, 107 (1987).
[6]S. Raman, C. H. Malarkey, W. T. Milner, C. W. Nester, and P. H. Stelson, At. Data Nucl. Data Tables **36**, 1 (1987), and references therein.
[7]J. H. Hamilton, P. G. Hansen, and E. F. Zganjar, Rep. Prog. Phys. **48**, 631 (1985), and references therein.
[8]*Proceedings of the International Workshop on Nuclear Structure in the Zr Region, Bad Honnef, 1988,* edited by J. Eberth, R. A. Meyer, and K. Sistemich (Springer-Verlag, Berlin, 1988).
[9]W. Nazarewicz, J. Dudek, R. Bengtsson, T. Bengtsson, and I. Ragnarsson, Nucl. Phys. **A435**, 397 (1985).
[10]R. Bengtsson, P. Moller, J. R. Nix, and Jing-ye Zhang, Phys. Scr. **29**, 402 (1984).
[11]J. H. Hamilton, A. V. Ramayya, C. F. Maguire, R. B. Piercy, R. Bengtsson, P. Moller, J. R. Nix, Jing-ye Zhang, R. L. Robinson, and S. Frauendorf, J. Phys. G **10**, 87 (1984).
[12]C. Thibault, F. Touchard, S. Buttgenbach, R. Klapisch, M. de Saint Simon, H. T. Duong, R. Jaquinot, P. Juncar, S. Liberman, P. Pillet, J. Pinard, J. L. Vialle, and A. Pesnelle, Nucl. Phys. **A367**, 1 (1981).
[13]M. Anselment, K. Bekk, S. Chonkum, S. Goring, A. Hanser, H. Hoeffgrn, W. Kalber, G. Meisel, and H. Rebel, Z. Phys. A **326**, 493 (1987).
[14]F. Buchinger, R. Corriveau, E. B. Ramsay, D. Berdichevsky, and D. W. L. Sprung, Phys. Rev. C **32**, 2058 (1985).
[15]A. G. Martin, S. B. Dutta, W. F. Rogers, and D. L. Clark, Phys. Rev. C **34**, 1120 (1986).
[16]D. A. Eastham, P. M. Walker, J. R. H. Smith, D. D. Warner, J. A. R. Griffith, D. E. Evans, S. A. Wells, M. J. Fawcett, and I. S. Grant, Phys. Rev. C **36**, 1583 (1987).
[17]K. Heilig and A. Steudel, At. Data Nucl. Data Tables **14**, 613 (1974).
[18]F. Buchinger, E. B. Ramsay, R. E. Silverans, P. Lievens, E. Arnold, W. Neu, R. Neugart, K. Wendt, and G. Ulm, Z. Phys. A **327**, 361 (1987).
[19]R. E. Silverans, P. Lievens, L. Vermeeren, E. Arnold, W. Neu, R. Neugart, K. Wendt, F. Buchinger, E. B. Ramsay, and G. Ulm, Phys. Rev. Lett. **60**, 2607 (1988).
[20]W. D. Myers and K. H. Schmidt, Nucl. Phys. **A410**, 61 (1983).
[21]F. Schussler, J. A. Pinston, E. Monnand, A. Moussa, G. Jung, E. Koglin, B. Pfeiffer, R. F. Janssens, and J. van Klinken, Nucl. Phys. **A339**, 415 (1980).
[22]R. E. Azuma, G. L. Borchert, L. C. Carraz, P. G. Hansen, B. Jonson, S. Matsson, O. B. Nilson, G. Nyman, I. Ragnarrson, and H. L. Ravn, Phys. Lett. **86B**, 5 (1979).
[23]C. J. Lister, B. J. Varley, H. G. Price, and J. W. Olness, Phys. Rev. Lett. **49**, 308 (1982).
[24]H. Ohm, G. Lhersonneau, K. Sistemich, B. Pfeiffer, and K. L. Kratz, Z. Phys. A **327**, 483 (1987).
[25]G. Lehersonneau *et al.* (unpublished).
[26]H. S. Kohler, Nucl. Phys. **A258**, 301 (1976).
[27]M. N. Butler, D. W. L. Sprung, and J. Martorell, Nucl. Phys. **A442**, 157 (1984).
[28]R. E. Silverans, P. Lievens, and L. Vermeeren, Nucl. Instrum. Methods **B26**, 591 (1987).
[29]A. C. Mueller, F. Buchinger, W. Klempt, E. W. Otten, R. Neugart, C. Ekstrom, and J. Heinemeier, Nucl. Phys. **A403**, 234 (1983).

[30]K. Wendt, S. A. Ahmad, F. Buchinger, A. C. Mueller, R. Neugart, and E. W. Otten, Z. Phys. A **318**, 125 (1984).
[31]H. L. Ravn and B. W. Allerdyce, CERN Rerpot No. CERN-EP/87-105 (1987).
[32]A. H. Wapstra and G. Audi, Nucl. Phys. **A432**, 1 (1985).
[33]V. S. Shirley and C. M. Lederer, *Table of Isotopes,* 7th Ed. (Wiley, New York, 1978).
[34]H. Kopfermann, *Nulcear Moments* (Academic, New York, 1958).
[35]W. H. King, J. Opt. Soc. Am. **53**, 638 (1963).
[36]M. Anselment, S. Chongkum, K. Bekk, S. Goring, A. Hausner, G. Meisel, and H. Rebel, Z. Phys. D **3**, 421 (1986).
[37]L. Olschewski, Z. Phys. **249**, 205 (1972).
[38]F. D. Feiock and W. R. Johnson, Phys. Rev. **187**, 39 (1969).
[39]P. A. Moskowitz and M. Lombardi, Phys. Lett. **46B**, 334 (1973).
[40]A. Bohr and V. F. Weisskopf, Phys. Rev. **77**, 94 (1950).
[41]M. Heider and O. Brink, Phys. Rev. A **16**, 1371 (1977).
[42]E. C. Seltzer, Phys. Rev. **188**, 1916 (1969).
[43]D. Bender, H. Brand, and V. Pfeuffer, Z. Phys. A **318**, 291 (1984).
[44]R. Engfer, H. Schneuwly, J. L. Uilleumier, H. K. Walter, and A. Zehnder, At. Data Nucl. Data Tables **14**, 509 (1974).
[45]C. Brechniac, S. Gerstenkorn, and P. Luc, Physica B+C **82C**, 409 (1976).
[46]G. Torbohm, B. Fricke, and A. Rosen, Phys. Rev. A **31**, 2038 (1985).
[47]J. Nag and M. K. Pal, Nucl. Phys. **A404**, 106 (1983).
[48]A. Arima and H. Horie, Prog. Theor. Phys. (Kyoto) **12**, 623 (1954).
[49]K. Heyde, J. Moreau, and M. Waroquier, Phys. Rev. C **29**, 1859 (1984).
[50]P. Moller and J. R. Nix, At. Data Nucl. Data Tables **26**, 165 (1981).
[51]K. Kumar, Phys. Lett. **28**, 249 (1972).
[52]L. Grodzins, Phys. Lett. **2**, No. 2, 88 (1962).
[53]D. Vautherin, Phys. Rev. C **7**, 296 (1973).
[54]D. Berdichevsky, R. Fleming, D. W. L. Sprung, and F. Tondeur, Z. Phys. A **329**, 393 (1988).
[55]D. W. L. Sprung, S. G. Lie, M. Vallieres, and P. Quentin, Nucl. Phys. **A326**, 37 (1979).
[56]O. Prior, F. Boehm, and S. G. Nilsson, Nucl. Phys. **A110**, 257 (1968).
[57]E. Moya de Guerra, Phys. Rep. C **138**, 293 (1986).
[58]F. Villars, Proceedings of the International School of Physics "Enrico Fermi," Course XXXVI, Varenna, 1986, edited by C. Bloch (Academic, New York, 1966).
[59]I. Ragnarsson, and R. K. Sheline, Phys. Scr. **29**, 385 (1984).
[60]X. Campi and M. Epherre, Phys. Rev. C **22**, 2605 (1980).
[61]X. Campi, D. W. L. Sprung, and J. Martorell, Nucl. Phys. **A223**, 541 (1974).
[62]M. Sakai, At. Data Nucl. Data Tables **31**, 399 (1984).
[63]A. DeShalit and M. Goldhaber, Phys. Rev. **92**, 1211 (1953).
[64]D. Berdichevsky and U. Mosel, Nucl. Phys. **A338**, 205 (1982).
[65]D. Berdichevsky, J. Phys.C **6**, 221 (1984).